Metal-Organic Framework MIL-68(In)-NH_2 on the Membrane Test Bench for Dye Removal and Carbon Capture

Bahram Hosseini Monjezi[1], Benedikt Sapotta[1], Sarah Moulai[1], Jinju Zhang[2], Robert Oestreich[3], Bradley P. Ladewig[2], Klaus Müller-Buschbaum[4,5], Christoph Janiak[3], Tawheed Hashem[1,*], and Alexander Knebel[1,6,*]

DOI: 10.1002/cite.202100117

Supporting Information available online

Dedicated to Prof. Dr. rer. nat. Jürgen Caro on the occasion of his 70th birthday

The metal-organic framework (MOF) MIL-68(In)-NH_2 was tested for dye removal from wastewater and carbon capture gas separation. MIL-68(In)-NH_2 was synthesized as a neat, supported MOF thin film membrane and as spherical particles using pyridine as a modulator to shape the morphology. The neat MIL-68(In)-NH_2 membranes were employed for dye removal in cross-flow geometry, demonstrating strong molecular sieving. MIL-68(In)-NH_2 particles were used for electrospinning of poylethersulfone mixed-matrix membranes, applied in dead-end filtration with unprecedented adsorption values. Additionally, the neat MOF membranes were used for H_2/CO_2 and CO_2/CH_4 separation.

Keywords: Carbon capture, Dye removal, Metal-organic frameworks, Molecular sieving membranes, Nanofiltration

Received: June 18, 2021; *revised:* November 04, 2021; *accepted:* December 07, 2021

1 Introduction

Metal-organic frameworks (MOFs) are porous, highly versatile, and tailorable hybrid materials, widely explored for separations [1]. In particular, MOF-based membranes have demonstrated great potential for the separation of gases, liquids, ions, and other important separation tasks [2–4]. MOFs are employed as membranes following different material concepts: 1) They can be synthesized on ceramic supports, e.g., α-Al_2O_3) as neat-MOF membranes by solvothermal methods or in a layer-by-layer fashion, yielding intergrown polycrystalline thin films [5–7]. Or 2) they can be incorporated as MOF (nano)particles into polymeric matrices and fabricated into mixed-matrix membranes (MMMs) [2, 8, 9]. Membrane technology itself is as versatile as the MOFs chemistry [10, 11]. Membranes find applications in sensor technology, in Li-ion batteries as separator, and in fuel cells as ion-conducting membranes [12–15]. Membranes are already used for different applications: in gas separation industry for CO_2 removal from natural gas, N_2/O_2 separation, or H_2 recovery [10, 11]; and, also, in the oil and gas sector, in hydrocarbon purification, membranes are important, whereas cryogenic distillation is still the main technique here [1]. For water treatment, mainly

[1]Bahram Hosseini Monjezi, Benedikt Sapotta, Sarah Moulai, Dr. Tawheed Hashem, Dr. Alexander Knebel
tawheed.hashem@kit.edu
Institute of Functional Interfaces (IFG), Karlsruhe Institute of Technology (KIT), Hermann-von-Helmholtz Platz 1, 76344 Eggenstein-Leopoldshafen, Germany.

[2]Dr. Jinju Zhang, Dr. Bradley P. Ladewig
Institute for Micro Process Engineering (IMVT), Karlsruhe Institute of Technology (KIT), Hermann-von-Helmholtz Platz 1, 76344 Eggenstein-Leopoldshafen, Germany.

[3]Robert Oestreich, Prof. Dr. Christoph Janiak
Institute for Inorganic and Structural Chemistry, Heinrich-Heine-University Düsseldorf, Universitätsstraße 1, 40225 Düsseldorf, Germany.

[4]Prof. Dr. Klaus Müller-Buschbaum
Institute of Inorganic and Analytical Chemistry, Justus-Liebig-University Giessen, Heinrich-Buff-Ring 17, 35392 Giessen, Germany.

[5]Prof. Dr. Klaus Müller-Buschbaum
Center of Materials Science (LAMA), Justus-Liebig-University Giessen, Heinrich-Buff-Ring 16, 35392 Giessen, Germany.

[6]Dr. Alexander Knebel
alexander.knebel@uni-jena.de
Otto Schott Institute of Materials Research, Friedrich Schiller University Jena, Fraunhoferstraße 6, 07743 Jena, Germany.

desalination via reverse-osmosis is practically used, but wastewater treatment and nanofiltration applications are also gaining interest [16–19]. Membranes are widely applied, and by the addition of MOFs that boost their performance, they have the potential to assist in critical global tasks, such as establishing a circular CO_2 economy, purifying drinking water, and producing biofuels, e.g., biomethane [20]. They could also be used in green and renewable hydrogen processes [21–23]. For instance, MOFs have already been extensively investigated as adsorbents for water capture from air [24]. This work was conducted as a result of a combination of MOF-based membranes and novel separation approaches. The separations demonstrated herein consist of dead-end and cross-flow [16] setups to test dye removal from wastewater, whereas the Wicke-Kallenbach technique is utilized to perform gas separation membrane testing for carbon capture applications [13]. All devices and their working principles are shown in Fig. 1.

In the first part of this paper, the focus is mainly on the continuous cross-flow separation of two dyes of different size from aqueous solution by a molecular sieving approach. Slight differences in the size of molecules can make a huge deviation in separation properties, especially for continuous separations. In the second part, the adsorptive removal of the small dye methylene blue (MB) by dead-end filtration is examined. Finally, the continuous carbon capture gas separation using the Wicke-Kallenbach techniquesis investigated. A variety of MOFs and MOF-based mixed-matrix membranes have been shown to be effective at removing dyes from wastewater. Here, it is shown that NH_2MIL-68(In), an indium-based Kagomé MOF with giant channels of ~7 Å and ~20 Å diameter, with its amino-functionalized linkers (Fig. 2) [25], shows unprecedented strong adsorption for dyes over water in MMMs as well as long-term stability in molecular sieving of dyes from water. The generally low toxicity of indium to the human body accompanied with zero leaching from the MOF itself makes this MOF a very important candidate for wastewater treatment [3, 25–27].

MIL-68(In)-NH_2 has also been shown to have highly suitable adsorption properties for the desired applications, mainly because of the amino-group functions as an electrostatic interaction site for CO_2 and its hydrophilicity [7, 28]. It was expected to show high performance, especially for wastewater treatment by dye separation. Wastewater treatment with a focus on the separation of organic dye molecules is a highly important topic, due to the high toxicity of dye molecules when taken up by the human body. Especially in third-world countries, the pollution of rivers with dyes from textile industries is a big issue [29]. To tackle the dye pollution of water, neat MIL-68-NH_2 membranes on ceramic supports in cross-flow geometry are tested. These neat MIL-68(In)-NH_2 membranes have been prepared solvothermally on an α-Al_2O_3 support. Due to their promising performance, they were also tested for gas separation with binary mixtures of H_2/CO_2 and CO_2/CH_4. However, the adsorptive properties of MIL-68(In)-NH_2 are of highest interest here, as it is a giant pore MOF. Therefore, electrospun mixed-matrix membranes with different wt % of MIL-68(In)-NH_2 were prepared to be tested in adsorptive separation. The MOF pore walls should favor adsorption of polar species, such as anionic or cationic dyes, but

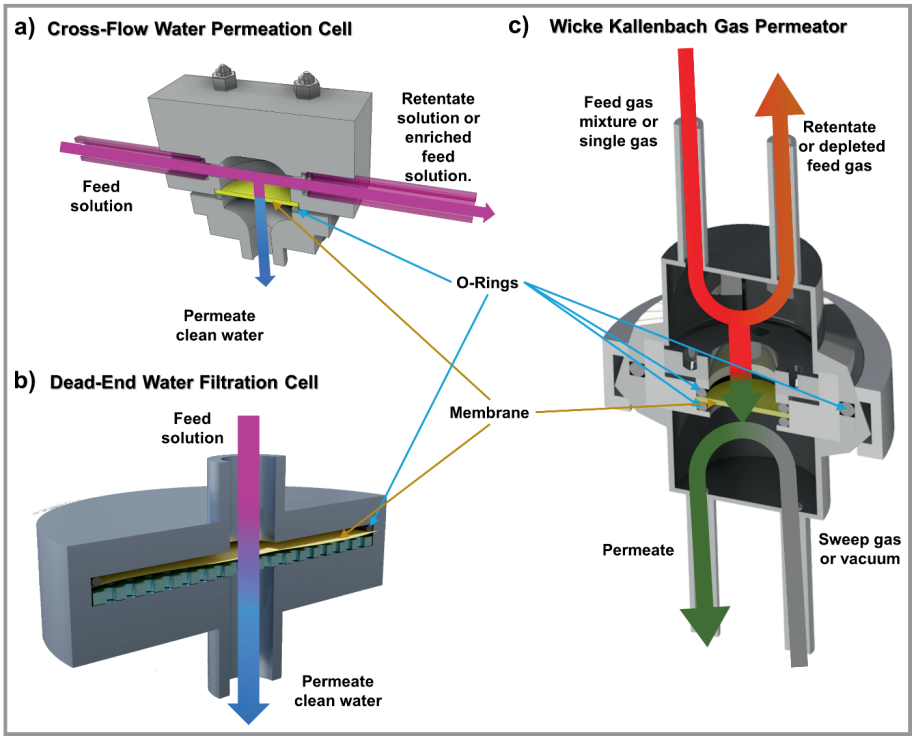

Figure 1. Half-section images of the separation techniques used in this study: a) cross-flow device for continuous wastewater treatment technology, b) the dead-end module, and c) Wicke-Kallenbach gas permeator for gas separation.

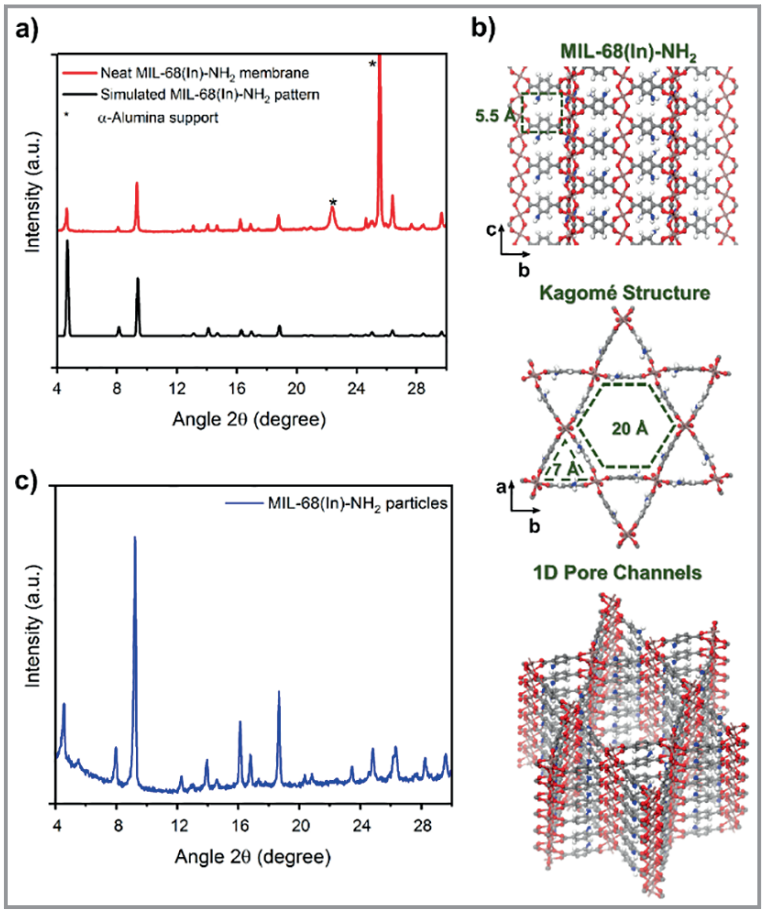

Figure 2. a) X-ray diffraction (XRD) of the supported MIL-68(In)-NH_2 membrane thin film for dye rejection and gas separation measurements and a simulated powder XRD (PXRD) pattern (CCDC 1824633). b) Structural properties of the Kagomé MOF MIL-68(In)-NH_2 with focus on pore sizes (C, gray; In, orange; O, red; N, blue; H, white). c) PXRD of the MIL-68(In)-NH_2 particles used for mixed-matrix membranes in this study.

also that of quadrupolar CO_2, mainly because of the NH_2 group [7, 28, 30].

2 Experimental Section

2.1 Synthetic Conditions

All chemicals were used as received. Deionized water was used in all cases. Methylene blue, *N*-methyl-2-pyrrolidone (NMP), pyridine (anhydrous), and rose bengal (85 %) were purchased from Merck, whereas acid fuchsin (≥ 60 %) and 2-aminoterephthalic acid (NH_2-$BDCH_2$, 99 %) were supplied by Acros Organics. *N*,*N*-dimethylformamide (DMF, ≥ 99.9 %, anhydrous) was obtained from VWR, $In(NO_3)_3{\cdot}H_2O$ (99.99 %) was supplied by Alfa Aesar, and polyethersulfone (PES) was purchased from Goodfellow. The asymmetric α-Al_2O_3 membrane supports with 70-nm grain top-layer were purchased from Fraunhofer IKTS.

MIL-68(In)-NH_2 powder was prepared solvothermally, with slight variations from the literature [25]. In a typical synthesis procedure, 1.92 mmol of $In(NO_3)_3{\cdot}xH_2O$ and 0.645 mmol of NH_2-$BDCH_2$ were dissolved in 6.2 mL DMF in a Teflon (polytetrafluoroethylene, PTFE)-lined autoclave. After adding 0.225 mL pyridine and stirring for 15 min, the autoclave was sealed and kept at 125 °C for 5 h. The resulting yellowish powder was washed with fresh DMF and dried in a Leica EM CPD300 CO_2 critical point dryer. Further synthesis parameters are given in the Supporting Information (Sect. S1, Tab. S1, and Fig. S1). To synthesize MIL-68(In)-NH_2 membranes, the α-Al_2O_3 membrane support was placed in a homemade PTFE holder face-down in a PTFE-lined autoclave. The same chemicals and amounts were used for membrane synthesis. After synthesis, the film was solvent-exchanged with fresh DMF over 24 h and dried afterward at 80 °C under air.

MMMs were prepared through a simple electrospinning procedure in a slight variation from ref. [31]. PES powder was dissolved in a mixture of 80 % DMF and 20 % NMP (variation from [32]) and stirred for 2 h at room temperature. MIL-68(In)-NH_2 powder was added to the PES solution at ratios of 5, 10, and 15 wt % to yield 1 g of composite. PES@MIL-68-NH_2 solution was ultrasonicated for 30 min and then stirred overnight at 50 °C. The prepared solution was extruded by a syringe pump through a capillary tip with a diameter of 0.5 mm. The stainless-steel spinneret was the positive electrode. The optimum electrospinning parameters were applied voltage of 19 kV, flow rate of 0.1 mL h^{-1}, and tip-to-collector distance (TCD) of 18 cm. After spinning, a phase inversion technique was used to finish the polymer membrane in a water bath for 2 h. The membrane was rinsed with deionized water and dried at room temperature for 24 h.

2.2 Techniques

Dye rejection performance of the MIL-68(In)-NH_2 membranes was determined by nanofiltration with a custom-made cross-flow filtration device using a peristaltic pump. The effective membrane area was 706 mm^2. Using an aqueous dye stock solution of c_{feed} = 100 mg L^{-1}, pumped along the membrane, the retentate and permeate were recycled. The operating pressure was controlled at 0.1 MPa.

Dead-end dye removal was performed using an aqueous MB solution with initial concentrations of c_{feed} = 1 mg L^{-1}. The solutions were filtered through the membrane at a flow rate of 1 mL min^{-1} and 1 bar overpressure.

Single gas permeation was performed with a Wicke-Kallenbach apparatus using the pressure decay method. The downstream was held under vacuum with the upstream pressurized for 5 min to ensure the membrane was permeating at steady state, before the vacuum connection was closed and the consequent increase in downstream monitored with a digital manometer connected to a PC with LabVIEW software. The feed-side pressure for CO_2 was around 1.5 bar, while for CH_4 and H_2, it was 1.2 bar, at an operating temperature of 35 °C. Each membrane was tested three times, and their average permeation results are presented.

For (powder) X-ray diffraction ((P)XRD), a Bruker D8 ADVANCE AXS diffractometer with CuKα radiation (λ = 1.5418 Å) was used in θ-θ geometry, equipped with a LynxEye detector. The samples were investigated with a scan speed of 1 s and an increment of 0.02° per step.

For scanning electron microscopy (SEM), a TESCAN Vega 3 with a tungsten filament electron source was used. A working distance of 14 mm was set, with an emission voltage of 8–10 kV. Energy-dispersive X-ray spectroscopy (EDXS) and mapping (EDXM) were performed with a Bruker XFlash detector 610 M at an emission voltage of 10 kV. The samples were sputtered with a Bal-Tec MCS 010 coating system using an Au–Pd target prior to measurement.

UV-vis spectra were collected on a Cary5000 UV-vis spectrometer from Agilent Technologies to determine the dye concentration according to Lambert-Beer law and using a series of pre-measured standard solutions.

3 Results and Discussion

3.1 MIL-68(In)-NH_2 Particle and Membrane Synthesis

In this work, MIL-68(In)-NH_2 was synthesized as particles and supported membrane. The MIL-68(In)-NH_2 with its orthorhombic structure and *Cmcm* space group [33] tends to grow in rod-shaped morphology, pyridine was added as a mild base, working as a modulator, leading to a decreased particle size. Additionally, it acts as a growth suppressor, yielding spherical to cubic-shaped materials instead of needles. MIL-68(In)-NH_2 is a Kagomé MOF showing the characteristic star shape in the a-b lattice-plane. At first glance, MIL-68(In)-NH_2 appears to have only 1D pores, but in the a and c and a-b direction, there are small pore openings with a diameter of 5.5 Å. This makes it a 3D porous framework accessible for small molecules, such as H_2, CO_2, and CH_4 with kinetic diameters of 2.9, 3.3, and 3.8 Å, respectively. The MIL-68(In)-NH_2 framework exhibits three types of pore windows of various geometries with average openings of 5.5 Å (cubic), 7 Å (trigonal), and 20 Å (hexagonal). For each average pore opening, a deviation from average can be assumed to be ±2 Å because of the rotational freedom of the benzene rings (gate-opening/closing, linker swing [34]). Nevertheless, the pore openings are all large enough to allow diffusion in 3D space for the gases tested in this study and for H_2O (2.7 Å kinetic diameter). Fig. 2 displays the PXRD of the supported membrane film and PXRD data of the used MIL-68(In)-NH_2 powders in comparison to a simulated PXRD pattern. From simulation, it is observed that the obtained particles reveal a deviation from the common needle shape of MIL-68(In)-NH_2 towards a cube-shaped morphology (c.f. Figs. 2 a and b). The crystallinity of the particles and the membrane is similarly high.

In Fig. 3a, the cross-sectional SEM of the α-Al_2O_3-supported MIL-68(In)-NH_2 membrane is shown. A homogeneous and continuous MOF layer of approximately 2 µm thickness is obtained from synthesis, which shows barely any particulate on top of the film. It is a densely intergrown film with grain sizes of about 500 nm. The corresponding EDXM in Fig. 3b in combination with PXRD data from Fig. 2a is assumed to be the MIL-68(In)-NH_2 film. The C signal (red) is distributed everywhere, making it unclear to assign to MIL-68(In)-NH_2. The In signal (green), however, is very sharp and gives an idea of the MOF film and the dimension. The underlying α-Al_2O_3 is shown as signal of the Al (blue) in the map color mixture. In Fig. 3c, a shot of the cross section and surface is taken at a stage tilt angle of 35°. The surface morphology is found to be overall rough, but densely intergrown without any pinholes or defects, e.g., cracks.

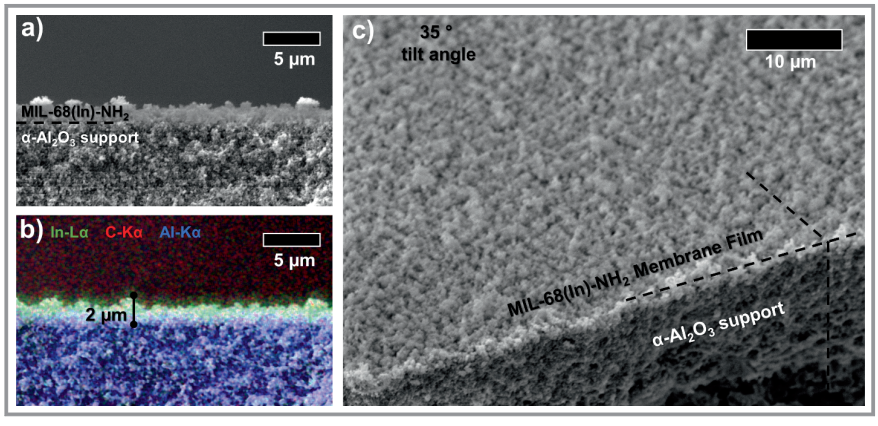

Figure 3. a) Cross section SEM analysis of the as-synthesized supported MIL-68(In)-NH_2 membrane on α-Al_2O_3. b) Energy-dispersive X-ray spectroscopic mapping of the cross section with signals for In (green), C (red), and Al (blue). c) SEM image in 35° tilt angle; full and homogeneous coverage with MIL-68(In)-NH_2 is observed.

3.2 Cross-Flow Dye Rejection

This neat, supported MIL-68(In)-NH_2 membrane was used in a cross-flow cell (c.f. Fig. 1a) for wastewater treatment of 100 mg L^{-1} dye stock solutions, either of rose bengal or acid fuchsin. Therefore, the solution was pumped with 1 bar overpressure from a large reservoir towards the membrane. Here, the permeate is the clean water passing the membrane film, whereas the enriched retentate is fed back to the large stock solution reservoir. Due to the small membrane area and low amount of permeate in contrast to the reservoir, it is assumed that the stock-solution concentration does not change during the separation process. Excess of permeate that was not needed for measurements was added back to the solution. The extinction of the permeate was measured with UV-vis and concentrations were calculated using diluted stock solutions for the linear absorption regime and Lambert-Beers law.

The separation data of the cross-flow filtration is recorded over 96 h of continuous run time after the equilibrium state was reached, to show long-term stability of the separation values (c.f. Fig. 4). The average data is shown in Tab. 1. The permeance (P) through the membrane is given in Fig. 4a and the removal efficiency in Fig. 4b. Also, the water permeance of the α-Al_2O_3 support is provided, which shows the highest possible permeance of P = 159.3 L $s^{-1}m^{-2}MPa^{-1}$. The water flux through the supported MIL-68(In)-NH_2 membrane of P = 125.1 L $s^{-1}m^{-2}MPa^{-1}$ is lowered by 22 % compared to the water flux of the bare support, indicating the dense intergrown nature of the membrane. The flux through the MIL-68(In)-NH_2 membrane strongly decreases depending on the dye: for acid fuchsin, the permeance is only P = 116.9 L $s^{-1}m^{-2}MPa^{-1}$, whereas for rose bengal, the permeance dropped to P = 75.9 L $s^{-1}m^{-2}MPa^{-1}$. An explanation for this behavior are the sizes and molecular weights (MW) of the dyes as given in Fig. 4c in comparison with the pore diameter of 20 Å of MIL-68(In)-NH_2. The pore diameter of MOF remains larger than the dye molecules, and therefore, a part of it can go through the membrane and block pores from water transport. This is also shown by the dye removal efficiency of the neat MIL-68(In)-NH_2 membrane in Fig. 4b.

The rejection of acid fuchsin by MIL-68(In)-NH_2 is 60 %, whereas for rose bengal it is 75.4 %. As the molecular size rises, the rejection rate increases, which is the usual behavior for molecular sieving. However, it must be considered for applications that water permeance can be lowered by small molecules that block the pores.

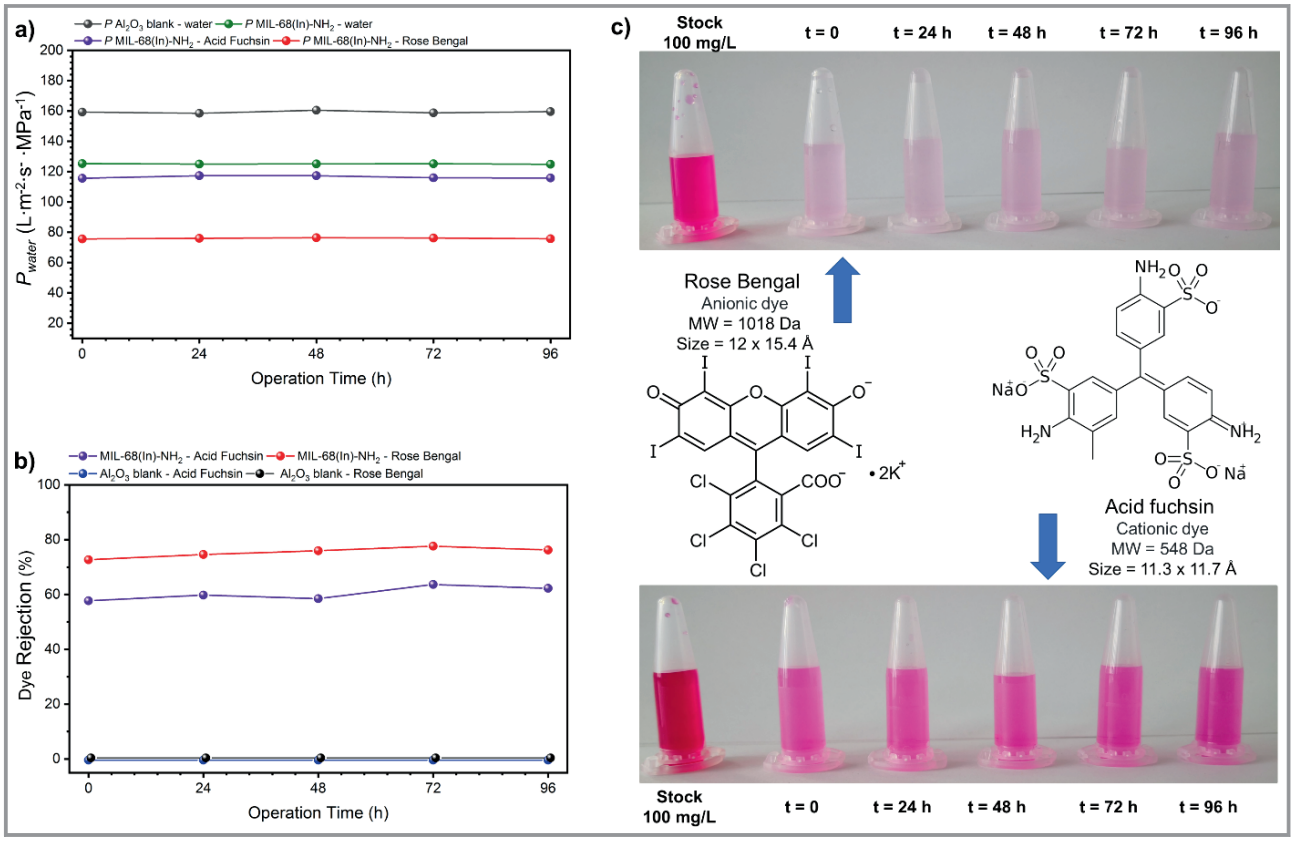

Figure 4. a) Water permeance over 96 h through the blank α-Al_2O_3 support and the supported MIL-68(In)-NH_2 membrane for pure water and dye solutions from rose bengal and acid fuchsin. b) Removal efficiency of the supported MIL-68(In)-NH_2 membrane. c) Photographs of the obtained solutions as well as Lewis formula and data of rose bengal and acid fuchsin.

Table 1. Cross-flow dye rejection and water permeance data.

Membrane	Dye solution	H_2O permeance [L $s^{-1}m^{-2}MPa^{-1}$]	Removal efficiency [%]
Al_2O_3-blank	water	159.3 ± 0.7	–
Al_2O_3-blank	acid fuchsin	159.3 ± 0.7	0
Al_2O_3-blank	rose bengal	159.3 ± 0.7	0
MIL-68-NH_2	water	125.1 ± 0.1	–
MIL-68-NH_2	acid fuchsin	116.9 ± 0.8	60 ± 2
MIL-68-NH_2	rose bengal	75.9 ± 0.3	75 ± 2

3.3 MMM Characterization and Dead-End Filtration

For dead-end filtration, electrospun PES fibre nanofiltration MMMs were prepared with 5, 10 and 15 wt % of MIL-68(In)-NH_2. These membranes are not dense films, they rather work as filters; here, the MOFs uptake is the important parameter. The small cationic dye MB was used as analyte and permeate concentrations are determined using UV-vis through Lambert-Beers law. In Figs. 5a and b, SEM images of the MIL-68(In)-NH_2 particles are shown. It is clearly visible that these particles have a spherical shape instead of a needle shape. They have a diameter of about 300 nm at a homogeneous size distribution. However, they can also be synthesized in a variety of morphologies (Fig. S1) by changing the reaction parameters. In Figs. 5c, d, e, and f, the resulting PES nanofiltration membranes are displayed in SEM images for neat PES, 5, 10, and 15 wt % MIL-68(In)-NH_2, respectively. The PES fibers are clearly visible, and the MIL-68(In)-NH_2 crystallites can be seen through the polymer fibers (best at 15 wt %). The spatial distributions of In, C, N, S, and O in PES@MIL-68(In)-NH_2 MMMs were shown by element mapping results and EDX spectrum (Fig. S2), demonstrating the presence of these elements in the final product. Surprisingly, with increasing wt % of MOF inside the fiber, the membranes show a better homogeneity, and less polymer droplet formation occurs. When comparing Fig. 5c, the neat polymer membrane being full of polymer droplets, with the 15 wt % MIL-68(In)-NH_2 membranes in Fig. 5f, a homogeneous fiber formation is evident for the latter.

To calculate the correct dye uptake values, the thickness of the membrane is important. Exemplarily, a cross section of a membrane with a loading of 10 wt % is shown in Figs. 5g and h. A 20° tilted cross section shows the surface morphology and homogeneous nature, the usual cross section is used to determine the thickness of the membrane, which is 35 µm here.

For dead-end dye removal measurements, the flow rate of the feed solution was adjusted to 1 mL min^{-1} and the initial concentration of the solution was c_{feed} = 1 mg L^{-1} of MB. The measurement was performed until the saturation of the membrane was clearly reached and then stopped. The derived data is shown in Fig. 6. All membranes show their performance very fast within the first 5 min of operation.

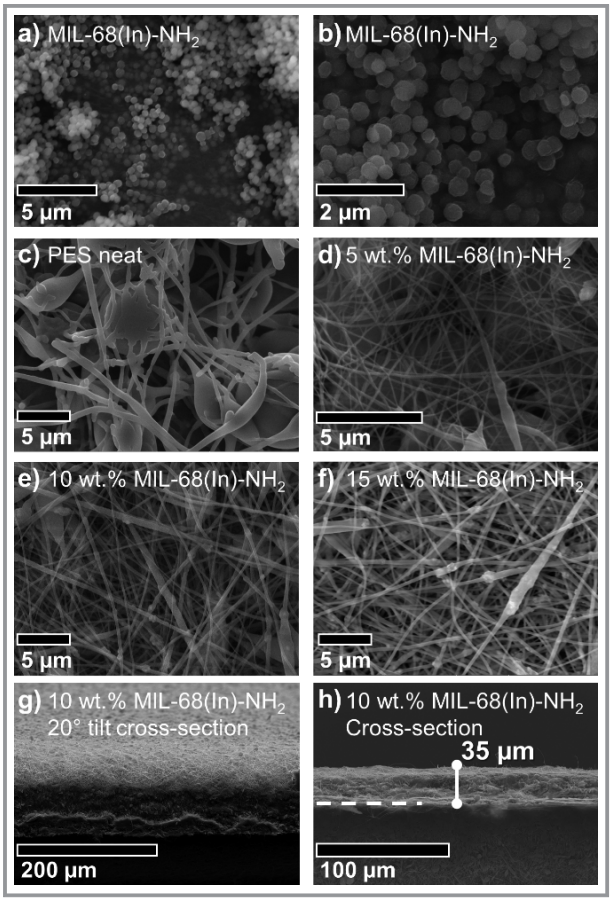

Figure 5. SEM images of membranes for dead-end filtration. a) MIL-68(In)-NH_2 particles, b) the same in higher resolution. The images show further c) neat PES fiber membranes and d), e), and f) the MIL-68(In)-NH_2 particles embedded in PES as MMMs with 5, 10, and 15 wt %, respectively. In g) 20° tilt angle and h) 0° angle cross-sectional images of the 10 wt % membrane are shown as examples.

As expected, higher wt % of MIL-68(In)-NH_2 mixed into the PES matrix yield high MB uptake (c.f. Fig. 6a). Interestingly, 5 wt % of MIL-68(In)-NH_2 does not differentiate very

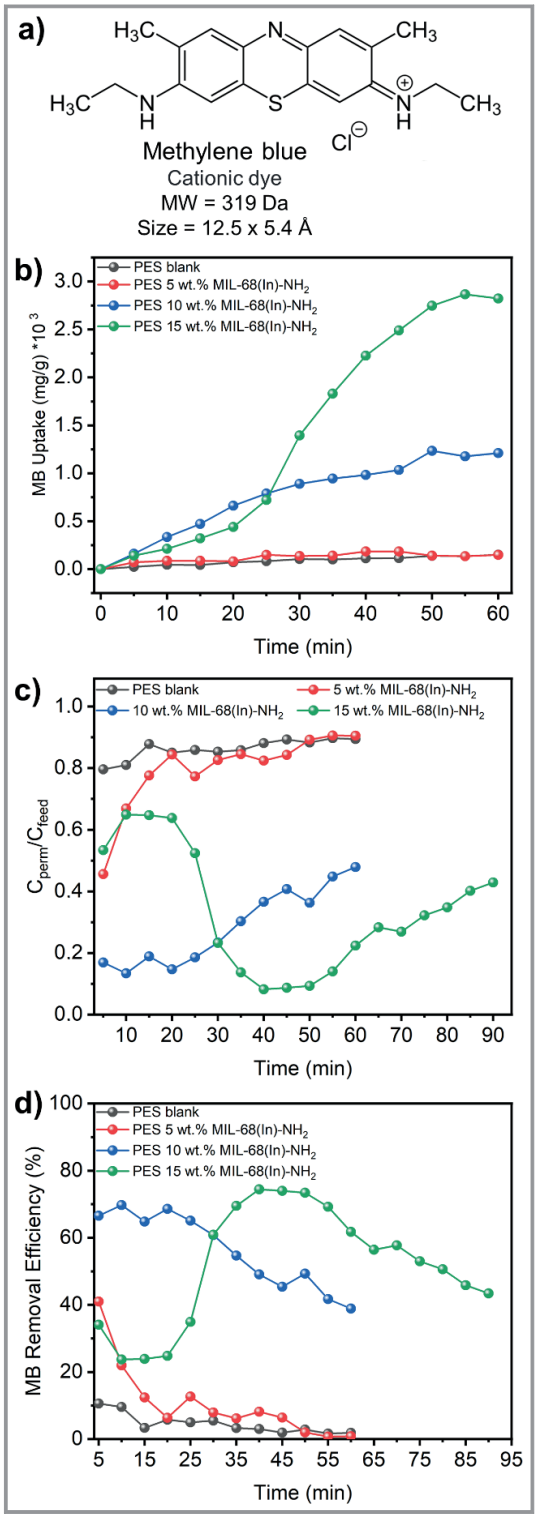

Figure 6. Dead-end MB removal data for neat PES and MMMs with 5, 10, and 15 wt % MIL-68(In)-NH_2. a) Lewis formula and data of MB, b) uptake over time, c) permeate vs feed concentration over time, and d) MB removal efficiency over time.

much from the neat PES membrane, whereas 10 wt % shows a good effect and 15 wt % shows a very outstanding effect of MB uptake up to 2822 mg g^{-1}, with on-line performance for over 20 min. As already discussed earlier, the membrane with 15 wt % seemed to work best with the electrospinning method. Notably, there seems to be a diffusion barrier for MB uptake into 15 wt % membrane for the first 25 min, as demonstrated by the concentration gradient graphic (concentration of permeate, c_{perm}, divided by concentration of feed, c_{feed}) or the removal efficiency graph (Figs. 6b and c). There is no easy explanation for this diffusion barrier; a change in polymer-filler interaction is assumed, as a surprisingly better fiber homogeneity was also found for the 15 wt % solution in the fiber spinning. The uptake into the 5 wt % MMM is very quick, and the removal efficiency diminishes after 20 min. For the 10 wt % MMM, the uptake is slow and steady, and the removal efficiency deteriorates gradually. However, for the 15 wt % MMM, the removal efficiency is low in the first place and starts to rise quickly and strong after 25 min operation time up to 75 %, remains there for 20 min until capacity is reached and then slowly declines.

For MIL-68(In)-NH_2, a very fast dye uptake to maximum capacity within 60 min was found and a capacity of up to 2822 mg g^{-1} for 15 wt % composite material. The uptake of the MIL-68(In)-NH_2 composites is ground-breaking and shows the highest uptake values among MOF-based materials. We have compared several reported values from literature with our values in Tab. S2. Only ZIF-8-graphene oxide and ZIF-8-carbon nanotube composites exceed the values of MIL-68(In)-NH_2 (see the Supporting Information). It is assumed that the amino function increases the uptake drastically, as it increases the hydrophilicity of the giant pore MIL-68(In)-NH_2. Additionally, the NH_2 group leads to a good polymer filler interaction with PES.

3.4 Gas Separation

The neat, supported MIL-68(In)-NH_2 membranes in Fig. 3 were investigated using the Wicke-Kallenbach technique with the pressure decay method for single gases. The results are shown in Fig. 7. As expected for this large pore MOF, the single gas permeances (in GPU (= 10^{-6} $cm^3cm^{-2}s^{-1}cm_{Hg}^{-1}$), gas permeation unit) are extraordinarily high with $P(CO_2)$ = $2 \cdot 10^{11}$ GPU, $P(CH_4)$ = $3 \cdot 10^{11}$ GPU and $P(H_2)$ = $4.5 \cdot 10^{11}$ GPU. However, the ideal separation factors are significantly lower, with $\alpha(H_2/CO_2)$ = 2.4 and $\alpha(CH_4/CO_2)$ = 1.4. Although the separation factors are above the Knudsen diffusion level, they are not competitive. It remained important to test the separation values for pure MOF membrane, as other studies reported extremely high separation values for MIL-68(Al) in Matrimid®-based MMMs [8], and adsorptive separation of CO_2 for carbon capture was suggested for functionalized MIL-68 to be crucial and important [35]. The pure membrane, however, has been found not suitable for carbon capture.

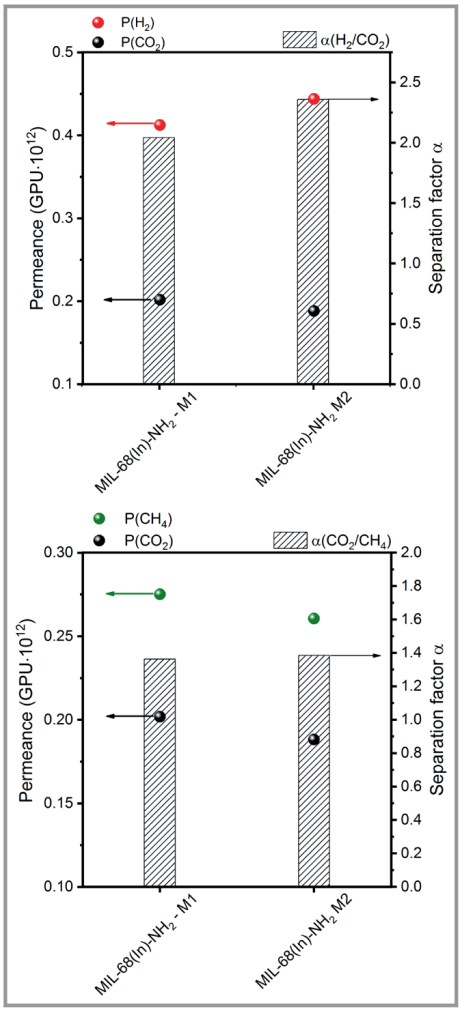

Figure 7. H_2/CO_2 (top) and CO_2/CH_4 separation (bottom). Single gas permeances and ideal separation factors for two identical supported MIL-68(In)-NH_2 membranes.

4 Conclusion

In our membrane tests, the large pore MOF MIL-68(In)-NH_2 has demonstrated excellent performance in organic dye separation. The removal of acid fuchsin and rose bengal from aqueous solution in cross-flow geometry yielded up to 75 % removal efficiency. High water fluxes up to $P = 125\,L\,s^{-1}m^{-2}MPa^{-1}$ were reached, but it was found that water permeance is dependent on the molecular size of dye molecules. Polyether sulfone composite membranes were produced, loaded with MIL-68(In)-NH_2 of up to 15 wt %. MMMs were tested in dead-end adsorptive methylene blue removal. They exhibit high removal performance, taking up to 2822 mg g^{-1} over operation times up to 60 min. In terms of gas separation, evaluated by the Wicke-Kallenbach technique and single gases, MIL-68(In)-NH_2 does not perform very well. The very high gas permeance of up to $P(H_2) = 4.5 \cdot 10^{11}$ GPU was expected because of large pores; the low separation factors of $\alpha(H_2/CO_2) = 2.4$ and $\alpha(CH_4/CO_2) = 1.4$ were measured. Overall, the MIL-68(In)-NH_2 framework has shown to be a very suitable candidate for dye removal wastewater treatment, because of its high uptake values, 96-h stability in operando and high removal rates. For future work, MIL-68(In)-NH_2 could be considered for the cross-flow separation of larger molecules. The molecular gate has been bigger than the dye molecules used in this study, so that it is rather suitable for separation or purification of hormones or proteins. However, the adsorptive separation of small species over water is extremely good. MIL-68(In)-NH_2 is definitely interesting for adsorptive separations of organic molecules and could also be tested for drug or hormone removal from wastewater.

Supporting Information

Supporting Information for this article can be found under DOI: https://doi.org/10.1002/cite.202100117. This section includes additional references to primary literature relevant for this research [36–70].

A. Knebel, B. Hosseini Monjezi, C. Janiak, K. Müller-Buschbaum, and R. Oestreich acknowledge funding through the Deutsche Forschungsgemeinschaft (DFG) within the Priority Program SPP 1928/2 COORNETs. A. Knebel acknowledges funding through the Carl Zeiss Foundation Breakthrough Program. T. Hashem and B. Sapotta acknowledge support through the Deutsche Forschungsgemeinschaft (DFG) within the Cluster "3DMM2O" funded by Germany's Excellence Strategy – 2082/1 – 390761711. Open access funding enabled and organized by Projekt DEAL.

Symbols used

c	[kg L^{-1}]	concentration
p	[Pa]	pressure
P	[L $s^{-1}m^{-2}MPa^{-1}$]	water permeance
TCD	[m]	tip-to-collector distance
α	[–]	separation factor

Abbreviations

α-Al_2O_3	alpha alumina
CCDC	Cambridge Crystallographic Data Centre
DMF	*N*,*N*-dimethylformamide
EDXM	energy-dispersive X-ray spectroscopy mapping
EDXS	energy-dispersive X-ray spectroscopy
MB	Methylene blue
MIL-68(In)-NH_2	Matériaux de l'Institut Lavoisier number 68 with indium and amino-function

MMM	mixed-matrix membrane
MOF	metal-organic framework
NH_2-$BDCH_2$	2-aminoterephthalic acid
NMP	*N*-methyl-2-pyrrolidone
PES	polyethersulfone
PTFE	polytetrafluoroethylene (Teflon®)
PXRD	powder X-ray diffraction
SEM	scanning electron microscopy
UV-vis	ultraviolet-visible spectroscopy
XRD	X-ray diffraction

References

[1] B. Hosseini Monjezi, K. Kutonova, M. Tsotsalas, S. Henke, A. Knebel, *Angew. Chem., Int. Ed.* **2021**, *60 (28)*, 15153–15164. DOI: https://doi.org/10.1002/anie.202015790

[2] A. Knebel, A. Bavykina, S. J. Datta, L. Sundermann, L. Garzon-Tovar, Y. Lebedev, S. Durini, R. Ahmad, S. M. Kozlov, G. Shterk, M. Karunakaran, I. D. Carja, D. Simic, I. Weilert, M. Klüppel, U. Giese, L. Cavallo, M. Rueping, M. Eddaoudi, J. Caro, J. Gascon, *Nat. Mater.* **2020**, *19 (12)*, 1346–1353. DOI: https://doi.org/10.1038/s41563-020-0764-y

[3] Z. Wu, X. Yuan, H. Zhong, H. Wang, L. Jiang, G. Zeng, H. Wang, Z. Liu, Y. Li, *J. Mol. Liq.* **2017**, *247*, 215–229. DOI: https://doi.org/10.1016/j.molliq.2017.09.112

[4] J. Lu, H. Zhang, J. Hou, X. Li, X. Hu, Y. Hu, C. D. Easton, Q. Li, C. Sun, A. W. Thornton, M. R. Hill, X. Zhang, G. Jiang, J. Z. Liu, A. J. Hill, B. D. Freeman, L. Jiang, H. Wang, *Nat. Mater.* **2020**, *19 (7)*, 767–774. DOI: https://doi.org/10.1038/s41563-020-0634-7

[5] E. P. Valadez Sánchez, H. Gliemann, K. Haas-Santo, C. Wöll, R. Dittmeyer, *Chem. Ing. Tech.* **2016**, *88 (11)*, 1798–1805. DOI: https://doi.org/10.1002/cite.201600061

[6] E. P. Valadez Sánchez, A. Knebel, L. Izquierdo Sánchez, M. Klumpp, C. Wöll, R. Dittmeyer, *Langmuir* **2020**, *36 (29)*, 8444–8450. DOI: https://doi.org/10.1021/acs.langmuir.0c00875

[7] S. Friebe, A. Mundstock, D. Unruh, F. Renz, J. Caro, *J. Membr. Sci.* **2016**, *516*, 185–193. DOI: https://doi.org/10.1016/j.memsci.2016.06.015

[8] X. Dong, Q. Liu, A. Huang, *J. Appl. Polym. Sci.* **2016**, *133 (22)*, 43485. DOI: https://doi.org/10.1002/app.43485

[9] B. Seoane, V. Sebastián, C. Téllez, J. Coronas, *CrystEngComm* **2013**, *15 (45)*, 9483–9490. DOI: https://doi.org/10.1039/c3ce40847g

[10] J. Dechnik, C. J. Sumby, C. Janiak, *Cryst. Growth Des.* **2017**, *17 (8)*, 4467–4488. DOI: https://doi.org/10.1021/acs.cgd.7b00595

[11] J. Dechnik, J. Gascon, C. J. Doonan, C. Janiak, C. J. Sumby, *Angew. Chem., Int. Ed.* **2017**, *56 (32)*, 9292–9310. DOI: https://doi.org/10.1002/anie.201701109

[12] Y. Qiao, Y. He, S. Wu, K. Jiang, X. Li, S. Guo, P. He, H. Zhou, *ACS Energy Lett.* **2018**, *3 (2)*, 463–468. DOI: https://doi.org/10.1021/acsenergylett.8b00014

[13] J. M. Stangl, D. Dietrich, A. E. Sedykh, C. Janiak, K. Müller-Buschbaum, *J. Mater. Chem. C* **2018**, *6 (34)*, 9248–9257. DOI: https://doi.org/10.1039/C8TC01454J

[14] H. A. Patel, N. Mansor, S. Gadipelli, D. J. L. Brett, Z. Guo, *ACS Appl. Mater. Interfaces* **2016**, *8 (45)*, 30687–30691. DOI: https://doi.org/10.1021/acsami.6b12240

[15] A. B. Kanj, R. Verma, M. Liu, J. Helfferich, W. Wenzel, L. Heinke, *Nano Lett.* **2019**, *19 (3)*, 2114–2120. DOI: https://doi.org/10.1021/acs.nanolett.8b04694

[16] H. Fan, J. Gu, H. Meng, A. Knebel, J. Caro, *Angew. Chem., Int. Ed.* **2018**, *57 (15)*, 4083–4087. DOI: https://doi.org/10.1002/anie.201712816

[17] H. Fan, M. Peng, I. Strauss, A. Mundstock, H. Meng, J. Caro, *Nat. Commun.* **2021**, *12 (1)*, 38. DOI: https://doi.org/10.1038/s41467-020-20298-7

[18] S. Zhou, Y. Wei, L. Li, Y. Duan, Q. Hou, L. Zhang, L.-X. Ding, J. Xue, H. Wang, J. Caro, *Sci. Adv.* **2018**, *4 (10)*, eaau1393. DOI: https://doi.org/10.1126/sciadv.aau1393

[19] T. Hashem, A. H. Ibrahim, C. Wöll, M. H. Alkordi, *ACS Appl. Nano Mater.* **2019**, *2 (9)*, 5804–5808. DOI: https://doi.org/10.1021/acsanm.9b01263

[20] J. Daniel-Gromke, N. Rensberg, V. Denysenko, W. Stinner, T. Schmalfuß, M. Scheftelowitz, M. Nelles, J. Liebetrau, *Chem. Ing. Tech.* **2018**, *90 (1–2)*, 17–35. DOI: https://doi.org/10.1002/cite.201700077

[21] A. Trattner, M. Höglinger, M.-G. Macherhammer, M. Sartory, *Chem. Ing. Tech.* **2021**, *93 (4)*, 706–716. DOI: https://doi.org/10.1002/cite.202000197

[22] G. Avci, I. Erucar, S. Keskin, *ACS Appl. Mater. Interfaces* **2020**, *12 (37)*, 41567–41579. DOI: https://doi.org/10.1021/acsami.0c12330

[23] H. Asadi, A. Alizadehdakhel, A. Ramazani, F. Dorosti, *Polym. Bull.* **2021**, *78*, 6953–6968. DOI: https://doi.org/10.1007/s00289-020-03459-y

[24] N. Hanikel, M. S. Prévot, F. Fathieh, E. A. Kapustin, H. Lyu, H. Wang, N. J. Diercks, T. G. Glover, O. M. Yaghi, *ACS Cent. Sci.* **2019**, *5 (10)*, 1699–1706. DOI: https://doi.org/10.1021/acscentsci.9b00745

[25] C. Volkringer, M. Meddouri, T. Loiseau, N. Guillou, J. Marrot, G. Férey, M. Haouas, F. Taulelle, N. Audebrand, M. Latroche, *Inorg. Chem.* **2008**, *47 (24)*, 11892–11901. DOI: https://doi.org/10.1021/ic801624v

[26] C. Yang, J. Cheng, Y. Chen, Y. Hu, *RSC Adv.* **2016**, *6 (66)*, 61703–61706. DOI: https://doi.org/10.1039/C6RA09021D

[27] M. Saghanejhad Tehrani, R. Zare-Dorabei, *RSC Adv.* **2016**, *6 (33)*, 27416–27425. DOI: https://doi.org/10.1039/C5RA28052D

[28] L. Wu, M. Xue, S.-L. Qiu, G. Chaplais, A. Simon-Masseron, J. Patarin, *Microporous Mesoporous Mater.* **2012**, *157*, 75–81. DOI: https://doi.org/10.1016/j.micromeso.2011.12.034

[29] D. A. Yaseen, M. Scholz, *Int. J. Environ. Sci. Technol.* **2019**, *16 (2)*, 1193–1226. DOI: https://doi.org/10.1007/s13762-018-2130-z

[30] A. Khutia, C. Janiak, *Dalton Trans.* **2014**, *43 (3)*, 1338–1347. DOI: https://doi.org/10.1039/c3dt52365a

[31] Z. Tang, C. Qiu, J. R. McCutcheon, K. Yoon, H. Ma, D. Fang, E. Lee, C. Kopp, B. S. Hsiao, B. Chu, *J. Polym. Sci., Part B: Polym. Phys.* **2009**, *47 (22)*, 2288–2300. DOI: https://doi.org/10.1002/polb.21831

[32] G. Darko, A. Goethals, N. Torto, K. de Clerck, *Appl. Nanosci.* **2016**, *6 (6)*, 837–845. DOI: https://doi.org/10.1007/s13204-015-0504-9

[33] H. Amer Hamzah, W. J. Gee, P. R. Raithby, S. J. Teat, M. F. Mahon, A. D. Burrows, *Chem. – Eur. J.* **2018**, *24 (43)*, 11094–11102. DOI: https://doi.org/10.1002/chem.201801419

[34] B. Zheng, F. Fu, L. L. Wang, L. Yang, Y. Zhu, H. Du, *J. Phys. Chem. C* **2018**, *122 (13)*, 7203–7209. DOI: https://doi.org/10.1021/acs.jpcc.8b00018

[35] L. Wu, W. Wang, R. Liu, G. Wu, H. Chen, *R. Soc. Open Sci.* **2018**, *5 (12)*, 181378. DOI: https://doi.org/10.1098/rsos.181378

[36] Y. Li, Q. Du, T. Liu, X. Peng, J. Wang, J. Sun, Y. Wang, S. Wu, Z. Wang, Y. Xia, L. Xia, *Chem. Eng. Res. Des.* **2013**, *91*, 361–368.

[37] E. Haque, V. Lo, A. I. Minett, A. T. Harris, T. L. Church, *J. Mater. Chem. A* **2014**, *2*, 193–203.

[38] X. P. Luo, S. Y. Fu, Y. M. Du, J. Z. Guo, B. Li, *Microporous Mesoporous Mater.* **2017**, *237*, 268–274.

[39] Q. Chen, Q. He, M. Lv, Y. Xu, H. Yang, X. Liu, F. Wei, *Appl. Surf. Sci.* **2015**, *327*, 77–85.
[40] C. H. Lin, C. H. Gung, J. J. Sun, S. Y. Suen, *J. Membr. Sci.* **2014**, *471*, 285–298.
[41] B. Baheri, R. Ghahremani, M. Peydayesh, M. Shahverdi, T. Mohammadi, *Res. Chem. Intermed.* **2016**, *42*, 5309–5328.
[42] A. Aluigi, F. Rombaldoni, C. Tonetti, L. Jannoke, *J. Hazard. Mater.* **2014**, *268*, 156–165.
[43] Z. Sun, T. Feng, Z. Zhou, H. Wu, *e-Polym.* **2021**, *21*, 156–165.
[44] B. Zhao, Y. Wang, X. Li, B. Sun, Z. Jiang, C. Wang, *Colloid Surf., B* **2015**, *136*, 375–382.
[45] G. Crini, H. N. Peindy, *Dyes Pigm.* **2016**, *70*, 204–211.
[46] J. S. Yang, S. Y. Han, L. Yang, H. C. Zheng, *J. Chem. Technol. Biotechnol.* **2016**, *91*, 618–623.
[47] M. S. Tehrani, R. Zare-Dorabei, *Spectrochim. Acta, Part A* **2016**, *160*, 8–18.
[48] J. Abdi, M. Vossoughi, N. M. Mahmoodi, I. Alemzadeh, *Chem. Eng. J.* **2017**, *326*, 1145–1158.
[49] R. Zhang, S. Ji, N. Wang, L. Wang, G. Zhang, J. R. Li, *Angew. Chem., Int. Ed.* **2014**, *53*, 9775–9779.
[50] N. Wang, S. Ji, G. Zhang, J. Li, L. Wang, *Chem. Eng. J.* **2012**, *213*, 318–329.
[51] S. Yu, Z. Chen, Q. Cheng, Z. Lü, M. Liu, C. Gao, *Sep. Purif. Technol.* **2012**, *88*, 121–129.
[52] P. Daraei, S. Madaeni, E. Salehi, N. Ghaemi, H. S. Ghari, M. A. Khadivi, E. Rostami, *J. Membr. Sci.* **2013**, *436*, 97–108.
[53] H. Tang, S. Ji, L. Gong, H. Guo, G. Zhang, *Polym. Chem.* **2013**, *4*, 5621–5628.
[54] N. Wang, R. Zhang, T. Liu, H. Shen, S. Ji, J. R. Li, *AIChE J.* **2016**, *62*, 538–546.
[55] N. Wang, X. Li, L. Wang, L. Zhang, G. Zhang, S. Ji, *ACS Appl. Mater. Interfaces* **2016**, *8*, 21979–21983.
[56] L. Wang, M. Fang, J. Liu, J. He, L. Deng, J. Li, J. Lei, *RSC Adv.* **2015**, *5*, 50942–50954.
[57] Q. Chen, P. Yu, W. Huang, S. Yu, M. Liu, C. Gao, *J. Membr. Sci.* **2015**, *492*, 312–321.
[58] H. P. Srivastava, G. Arthanareeswaran, N. Anantharaman, V. M. Starov, *Desalination* **2011**, *282*, 87–94.
[59] L. Wang, N. Wang, G. Zhang, S. Ji, *AIChE J.* **2013**, *59*, 3834–3842.
[60] M. Liu, Q. Chen, K. Lu, W. Huang, Z. Lü, C. Zhou, S. Yu, C. Gao, *Sep. Purif. Technol.* **2017**, *173*, 135–143.
[61] J. Wang, L. Qin, J. Lin, J. Zhu, Y. Zhang, J. Liu, B. V. Bruggen, *Chem. Eng. J.* **2017**, *323*, 56–63.
[62] Y. Li, L. H. Wee, A. Volodin, J. A. Martens, I. F. J. Vankelecom, *Chem. Commun.* **2015**, *51*, 918–920.
[63] P. Chen, X. Ma, Z. Zhong, F. Zhang, W. Xing, Y. Fan, *Desalination* **2017**, *404*, 102–111.
[64] Y. Zhang, Y. Su, W. Chen, J. Peng, Y. Dong, Z. Jiang, *Ind. Eng. Chem. Res.* **2011**, *50*, 4678–4685.
[65] Y. Zhang, Y. Su, J. Peng, X. Zhao, J. Liu, J. Zhao, Z. Jiang, *J. Membr. Sci.* **2013**, *429*, 235–242.
[66] Q. Zhang, H. Wang, S. Zhang, L. Dai, *J. Membr. Sci.* **2011**, *375*, 191–197.
[67] A. V. R. Reddy, J. J. Trivedi, C. V. Devmurari, D. J. Mohan, P. Singh, A. P. Rao, S. V. Joshi, P. K. Ghosh, *Desalination* **2005**, *183*, 301–306.
[68] A. Akbari, S. Desclaux, J. C. Rouch, P. Aptel, J. C. Remigy, *J. Membr. Sci.* **2006**, *286*, 342–350.
[69] M. Amini, M. Arami, N. Mohammad, A. Akbari, *Desalination* **2011**, *267*, 107–113.
[70] S. U. Hong, M. L. Bruening, *J. Membr. Sci.* **2006**, *280*, 1–5.

